

Effect of Dynamic Strain Aging on Isothermal (473 K) Low Cycle Fatigue of Ferritic Ductile Cast Iron

Hayato Mouri^{1,*}, Morihito Hayashi² and Wilfried Wunderlich³

¹Graduate School of Science and Technology, Tokai University, Tokyo 181-0003, Japan

²Department of Mechanical Engineering, School of Engineering, Tokai University, Tokyo 181-0003, Japan

³Department of Material Science, School of Engineering, Tokai University, Tokyo 181-0003, Japan

The ferritic ductile iron (FCD400) is widely used as industrial material. As regards to its high temperature application, fatigue at elevated temperature, and advanced mechanical properties has been investigated and clarified. In low cycle fatigue (LCF), the S-N curve is presented by the relation of plastic strain to the number of cycles as fatigue life, which can be predicted by the Manson-Coffin model. In this model, the ductile index is appointed as a material constant of 0.5 and the ductile coefficient is related directly to the so-called plastic deformation capacity of the material. Namely, the low cycle fatigue life shall be dominated by the elongation rate. Concerned with it, one of authors reported that the elongation-to-fracture is 20% at room temperature, but reduces to about 9% at 473 K. This temperature is just within the range of dynamic strain ageing (DSA), which is the phenomenon of fluctuating stress due to mobile atoms in solid solution. So, in this study, strain controlled high temperature LCF-tests were carried out on ferritic cast iron at 473 K in air and the result is compared with those performed at room temperature, aiming to clarify the effect of elongation or DSA on the fatigue life. Particularly, this paper mentions about DSA effect to cyclic stress and cyclic plastic strain that causes contradiction of Manson-Coffin's model in "the plastic strain range versus number of cycles" and "the stress range versus number of cycles" between room temperature (293 K) and 473 K. The fatigue life time at 473 K is 175 cycles lower than that at 293 K for all stress levels. However, DSA phenomena did not occur at high strain in 473 K cyclic fatigue test although it cannot be observed in tensile tests at 473 K. Based on the Manson-Coffin rule, the parameters ($C_p = 0.09$ and 421, $n = 0.65$ and 0.89 at $T = 293$ and 473 K, respectively) for the fatigue life time prediction have been determined. [doi:10.2320/matertrans.MRA2008482]

(Received January 8, 2009; Accepted May 1, 2009; Published June 24, 2009)

Keywords: ductile cast iron, high temperature low-cycle-fatigue, plastic strain, elastic strain, total strain range, dynamic strain ageing

1. Introduction

Ferritic ductile cast iron (FCD400) is widely used as industrial material, because it has superior mechanical properties, such as excellent lubricate and ductility, as well as low price. It is also used as one of heat resistant materials for machinery parts applied at elevated temperatures. Therefore, advanced mechanical properties of ductile cast iron including fatigue at the isothermal heating have been recently investigated and clarified.¹⁻⁶⁾

The S-N curve of low cycle fatigue is presented by the relation of plastic strain to the number of cycles as fatigue life, which can be predicted by Coffin-Manson's model. In this model, the ductile index is appointed as a material constant of 0.5 and the ductile coefficient is related directly to the so-called plastic deformation capacity of the material. Namely, the low cycle fatigue life shall be dominated by the elongation rate. One of authors reported that the elongation is 20 and 9% at room temperature and 473 K, respectively.¹⁾ The brittleness at 473 K has been induced by a dynamic strain ageing (DSA), which is the phenomenon of fluctuating stress due to moving dislocations trapped by mobile solid solution atoms.

Thus, strain controlled low-cycle fatigue tests at high temperature have been carried out on ferritic cast iron. Particularly, this paper considers the influence of the DSA on cyclic stress and cyclic plastic strain which causes deviations of the Manson-Coffin's model in the plastic strain range versus number of cycles between 293 K and 473 K.

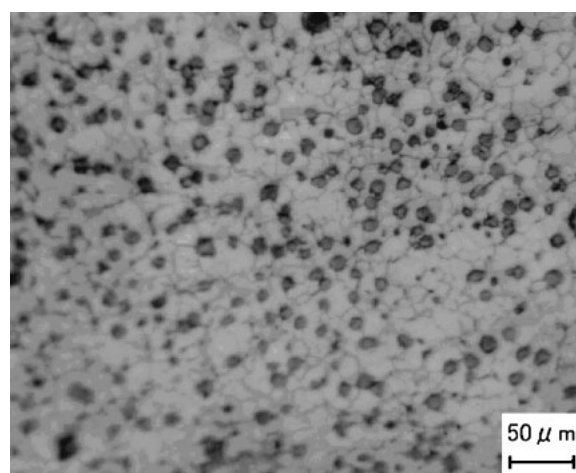


Fig. 1 Microstructure of ASTM 356 60-40-18/FCD400.

2. Experimental Procedure

2.1 Test material

Round test pieces (diameter 30 mm, length 210 mm) of FCD400 (Japan Industrial Standard) were used for the test. The chemical composition of specimen and microstructure of the transverse section is shown in Table 1 and Fig. 1. The tension test and fatigue test specimens were processed as shown in Fig. 2.

Figures 3 and 4 show the stress - strain diagram as obtained from the tensile test at 293 and 473 K, as black and hatched lines, respectively. The data are also shown in Table 2. So, it was confirmed that the test pieces lie within

*Graduate Student, Tokai University

Table 1 Chemical composition on ASTM 356 60-40-18/FCD400 (Chuo Malleable Iron Co., Ltd.).

Chemical composition (mass%)										
C	Si	Mn	P	S	Cr	Mg	Cu	Al	Sn	Fe
3.78	2.78	0.19	0.025	0.009	0.037	0.036	0.048	0.013	0.008	Balance

Table 2 Mechanical properties on FCD400 from tensile test (Strain rate: $\dot{\epsilon} = 0.4\%/s$).

	Specimen		FCD400 (JIS)	ASTM 356 60-40-18
	Temperature (K)			
Ultimate Tensile Strength (MPa)	293	473	400–500	400
0.2% Yield Strength (MPa)	476	411	Over 250	257
Elongation (%)	381	314	≥ 18	28
Rate of reduction (%)	20	8		
Young's ratio (Gpa)	13	16		
	235	101		

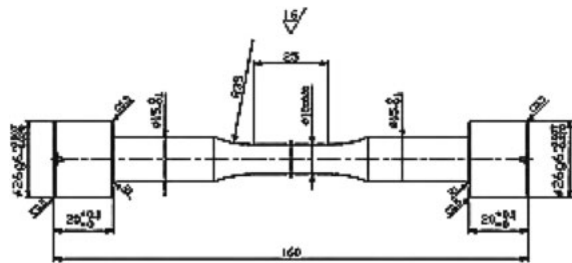


Fig. 2 Shape of fatigue specimen.

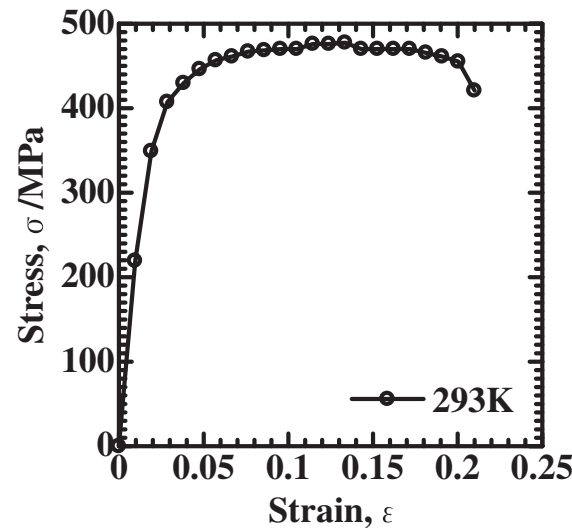


Fig. 3 Diagram of stress versus strain curve of ASTM 356 60-40-18/FCD400 at 293 K.

the range of the Japan Industrial Standard (JIS/ASTM 356 60-40-18).

2.2 Test condition

In this study, the high temperature low cycle fatigue tests were carried out by a computerized hydraulic servo pulsar EHF-ED100kN-TF-20L fabricated by Shimazu. The test was undertaken at 473 K, at a total strain range selected from

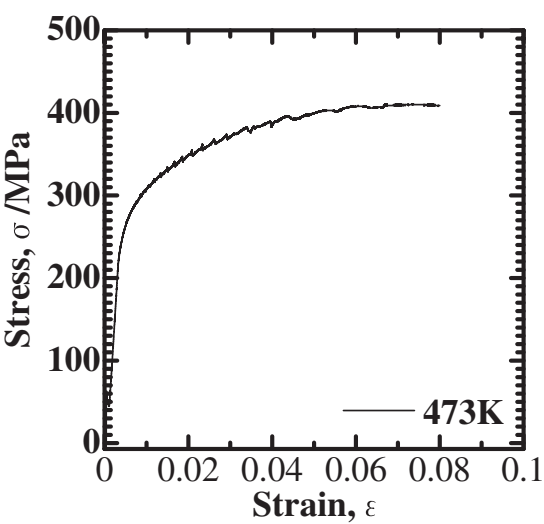


Fig. 4 Diagram of stress versus strain curve of ASTM 356 60-40-18/FCD400 at 473 K.

Table 3 Test Condition for low cycle fatigue.

Specimen	ASTM 356 60-40-18/JIS FCD400
Test environment	293 K and 473 K in Air
Wave form of strain	Triangular
Total strain range, $\epsilon_{tr}(\%)$	0.5–2
The rate of strain $\dot{\epsilon}$ (%/s)	0.4
Strain measurement	Displacement Sensor (GL = 15 mm)

0.5 to 2%, and at a constant strain rate of $0.4\%/s$ with triangular shaped cycles applied to specimens with gage length of 15 mm and diameter of 10 mm (Table 3). Test waveform is shown in Fig. 5. During test load, strain, number of repeated cycle and temperature of gage length were detected and recorded.

$$\dot{\epsilon} = 2\epsilon_{tr}/T = 2\epsilon_{tr}f \tag{1}$$

$\dot{\epsilon}$ [%/s] strain speed, ϵ_{tr} [%] total strain, $T[s]$ in the expression is the cycle period of the strain, and f is the frequency from eq. (1).

Table 4 Strain controlled low cycle fatigue test results of ASTM 356 60-40-18/FCD400. (waveform: saw tooth)

Speci.No.	f (Hz)	$\Delta\epsilon_t$ (%)	$\Delta\epsilon_t$ Actual (%)	$\Delta\epsilon_p$ (%)	$\Delta\epsilon_e$ (%)	σ_{\max} (MPa)	σ_{\min} (MPa)	σ_r (MPa)	σ_a (MPa)	N_f (Cycle)
473 (K)										
1	0.40	0.5	0.36	0.0070	0.5070	193	-238	431	216	247048
2	0.33	0.6	0.48	0.0492	0.5508	307	-342	649	324	24815
3	0.25	0.8	0.72	0.2357	0.5643	399	-424	823	412	4659
4	0.20	1	0.97	0.4221	0.5779	433	-455	888	444	2415
5	0.16	1.25	1.23	0.6768	0.5732	460	-480	940	470	1419
6	0.13	1.5	1.49	0.9315	0.5685	479	-497	976	488	990
7	0.11	1.75	1.74	1.1812	0.5688	493	-510	1002	501	757
8	0.10	2	2.00	1.4309	0.5691	504	-520	1024	512	404
Room Temperature										
17	0.40	0.5	0.36	0.0168	0.4832	302	-294	596	298	41396
18	0.33	0.6	0.46	0.0266	0.5734	316	-310	627	313	23649
19	0.25	0.8	0.72	0.1929	0.6071	380	-379	759	379	2119
20	0.20	1	0.97	0.4201	0.5799	404	-406	811	405	822
21	0.16	1.25	1.25	0.6921	0.5579	420	-424	844	422	447
22	0.13	1.5	1.51	0.9313	0.5687	430	-434	864	432	312
23	0.11	1.75	1.77	0.6795	0.5705	420	-423	843	421	458
24	0.10	2	2.02	1.4502	0.5498	444	-450	893	447	172
RT(FCD450 ³⁾)										
21	0.4	0.5		0.019	0.48	287	-291	578	289	67000
20	0.33	0.6		0.047	0.55	325	-352	677	339	18000
19	0.25	0.8		0.089	0.71	395	-413	808	338	8000
18	0.20	1		0.21	0.79	406	-420	825	413	1600
17	0.16	1.25		0.35	0.90	414	-425	839	419	730
16	0.13	1.5		0.52	0.98	424	-440	864	432	350
15	0.11	1.75		0.69	1.06	428	-449	878	439	200
14	0.1	2		1.15	0.85	437	-461	898	449	110

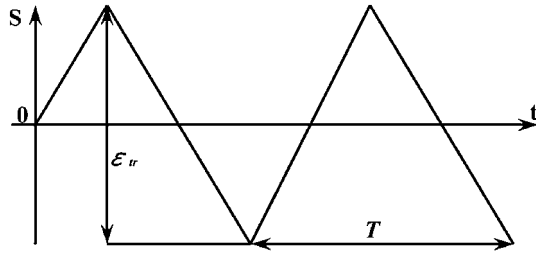


Fig. 5 Pulsating fast-fast wave for strain controlled fatigue test.

3. Results

3.1 Plastic strain and fatigue life

The plastic strain is obtained from the hysteresis loop to expression (2).

$$\epsilon_{tr} = \epsilon_{el} + \epsilon_{pl} \quad (2)$$

Strain controlled fatigue test results of FCD400 are shown in Table 4.

Figure 6 shows the relationship between plastic strain and fatigue life time. Rectangle dots are test performed at 293 K and triangle dots at 473 K. The fatigue life time at high plastic strain is longer at 473 K than at 293 K. On the other hand, fatigue life times at small plastic strains do not show large differences at all temperatures.

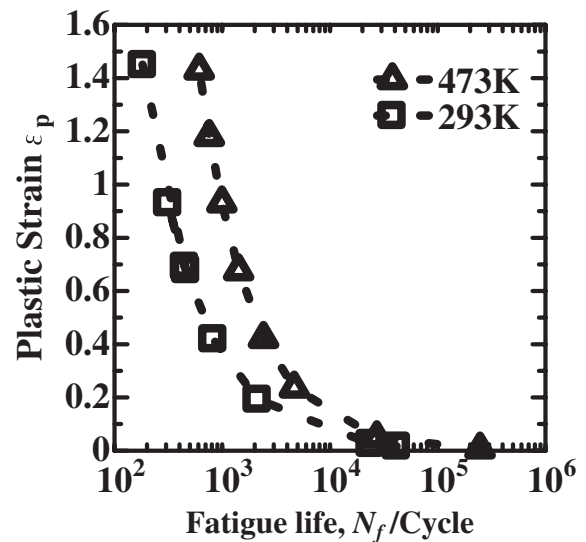


Fig. 6 Diagram of plastic strain versus fatigue life time for ASTM 356 60-40-18/FCD400.

3.2 Stress and fatigue life

Figure 7 shows the relationship between stress and fatigue life time. Rectangle dots refer to $T = 293$ K and triangle dots to $T = 473$ K. Specimens treated with large stress at 473 K have a longer life time than those at 293 K. When the stress

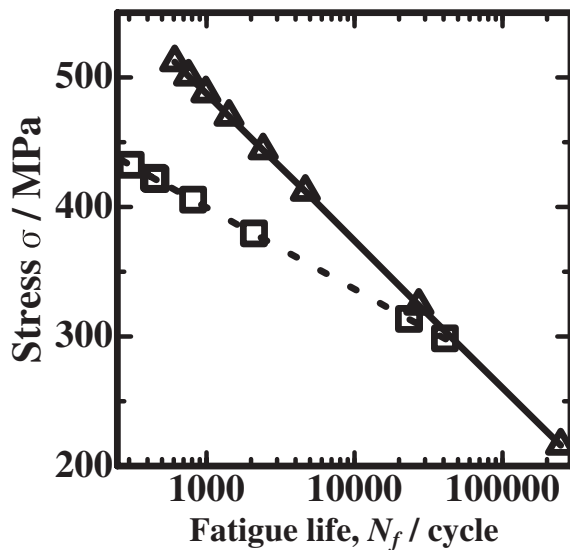


Fig. 7 Diagram of stress versus fatigue life time for ASTM 356 60-40-18/FCD400.

decreases, this behavior changes to the opposite and the crossing point is at 300 MPa.

3.3 Hysteresis loop

Figure 8 shows the hysteresis loop at the same stress level, but for different temperatures. Figure 8(a) shows 2% of Hysteresis loop. The stress of 2% hysteresis loop at 473 K is larger than at 293 K (Fig. 8(a)). Figure 8(b) shows the hysteresis loop at a stress level of 0.5%. The stress of the 0.5% hysteresis loop at 473 K is smaller than that at 293 K. Figures 8(c),(d) show larger magnifications of the 2% and 0.5% hysteresis loops. In both cases, there is small dynamic strain aging recognized at 473 K, but dynamic strain aging does not occur at 293 K.

3.4 Fractography

The fractography by SEM was also performed as seen in typical fractographs Fig. 9(a),(b) under the condition of 2% total strain. The photographs, taken after LCF experiments at two different temperatures, show the points of crack initiation, which occur at several locations on the surface at about 80% of the life time.

4. Discussion

4.1 About the relation between the plastic strain and the fatigue life

Normally, the fatigue life is calculated using the eq. (3)

$$\varepsilon_{pl} = C_p \cdot N_f^{\kappa_p} \quad (3)$$

with the parameters

$$C_p = 0.09, \kappa_p = 0.67 \text{ at } 293 \text{ K.}$$

This parameter set is valid for the temperature range, where no DSA effect occurs (293 K). At 473 K the steeper slope in Fig. 7 suggests these parameters are not valid any more: The fatigue life according to eq. (3) at a total strain of 2% would be 44 cycles, but in the experiment it is 404 cycles.

Because neither the index nor the coefficient includes the correct temperature dependence as in the experiment, a different set of parameters for the Manson-Coffin rule is necessary for the temperature range, where DSA occurs. All data can be fitted with negligible non-linear deviations at very high stresses with different sets of parameter as calculated according to eq. (3) as

$$C_p = 421, \kappa_p = 0.89 \text{ at } 473 \text{ K.}$$

Figure 6 showing the data at 473 K, are within the scattering and conform to each other. Such specimens have a significantly longer LCF life times than those at 293 K. Also the plastic strain of 473 K is larger than plastic strain at 293 K. These experimental data are different from normal behavior, where the fatigue life is short when the plastic strain is large. From Fig. 6 it is also deduced, that the fatigue life becomes almost the same in the case of low plastic strain independent of the temperature. It is considered that this behavior can be explained by less effective hardening: Dislocations are not yet pulled far enough to be fixed by carbon atoms, so that the Cottrell cloud is not yet formed; or in other words DSA is less occurring for small plastic strain.

4.2 Influencing factor to dynamic strain aging

For the confirmation of the presence of DSA, a tensile test at 473 K was also performed. The result is, that at the same strain rate $\dot{\varepsilon} = 0.4\%s^{-1}$ as in the fatigue experiments the DSA phenomenon occurs. However, when the tensile test was performed by interrupting a fatigue test of total strain of 2% after ten cycles at 473 K, DSA could not be confirmed. In this tensile test, the elongation until fracture was measured as 7%, smaller than that in a tensile test at virgin specimens (9%). Moreover, the yield stress is 428 MPa at tensile test after 162 fatigue cycles, but the yield stress at virgin specimens is almost 410 MPa. It is considered that the carbon atoms in solid solution are trapped in cores of immobile dislocations formed during the first fatigue cycles. Through this, mobile dislocations are not hindered anymore by carbon atoms and this explains the longer life time at high stress levels (Fig. 7) compared to 293 K.

4.3 About the relation between the stress and the fatigue life

Figure 7 shows the fatigue life time is 247048 cycles at a stress value of 216 MPa at 473 K, while at the same stress at 293 K 121187 cycles. Moreover, when the fatigue life at 512 MPa is compared, (172 cycles at 293 K, 404 cycles at 473 K) the life time increases. All data points are lying on a straight line, therefore the Manson-Coffin parameter can be estimated as shown above in (5). However, the data at 293 K are shifted towards shorter cycles. At 473 K all data are increases at 293 K about 57%.

4.4 Stress variation on hysteresis loop

The hysteresis loops in Fig. 8 were generated from the fatigue test data. At a total strain 2% (Fig. 8(a)) the maximum and minimum stresses at 293 K are almost constant, confirming a saturation, while at 473 K there is an inclined slope. The magnified curve in Fig. 8(c) confirmed that there

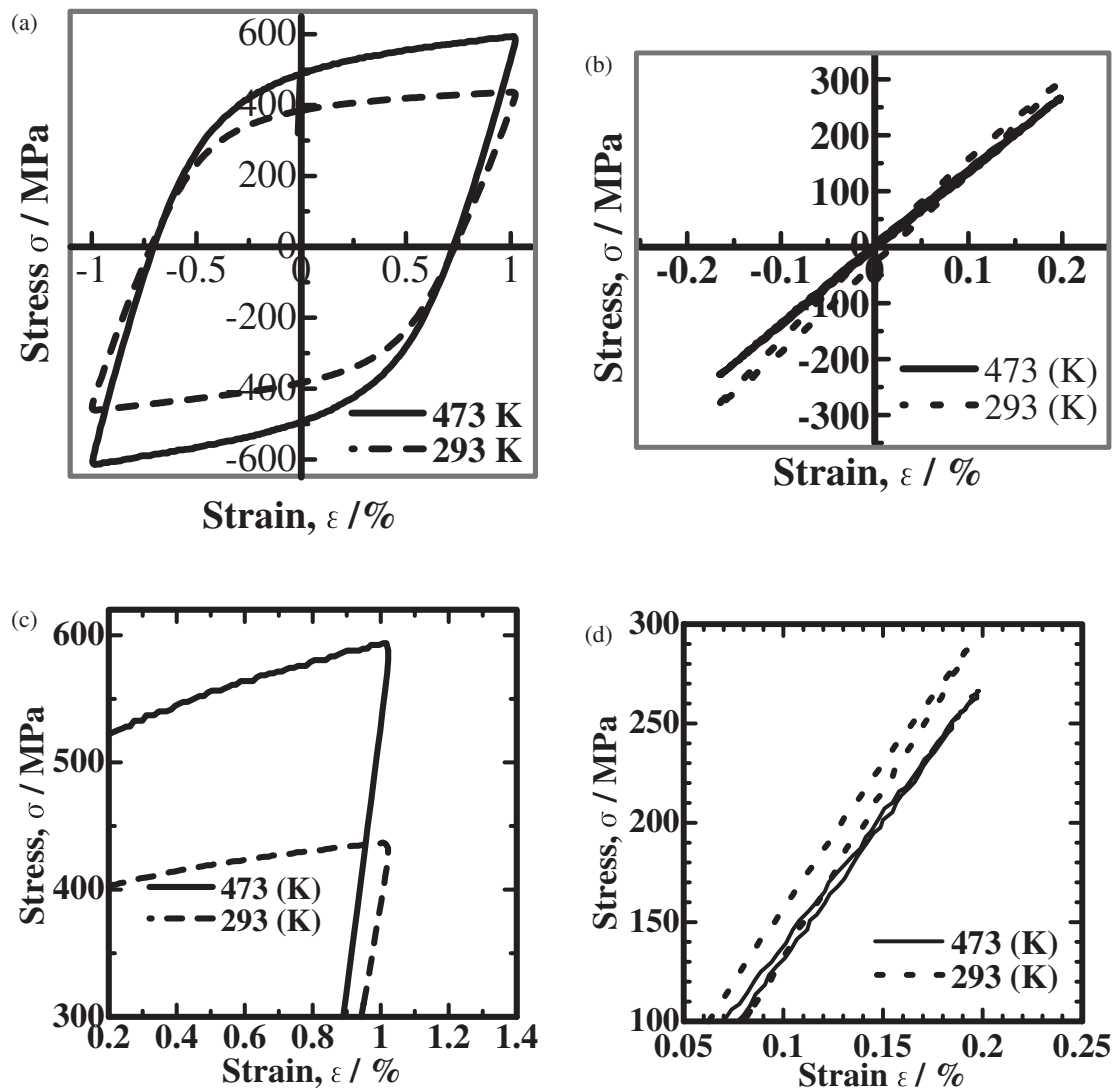


Fig. 8 Hysteresis loop at $N_f/2$ for LCF test with total plastic strain of (a) 2%, (b) 0.5%, (c),(d), enlargement of (a),(b) to clarify occurrence of DSA.

is no DSA phenomena at all three temperatures. However, at low total strain values (Fig. 8(b),(d)) the DSA behavior can be observed at 473 K.

4.5 Fractography

The fracture surfaces in all specimens are flat, perpendicular to the stress direction, indicating a mainly brittle manner of fracture. From the fractographies, it is deduced, that the interface to graphite particles is the initiation point of the crack because dimple pattern occur always around the particles. Dimple pattern, river pattern and striation have the same morphology at all temperature and also the coexistence of river pattern and striations could be confirmed in all cases (Fig. 9(a),(b)). The area, which is covered by striations, is larger for the specimens deformed at 0.5% of total strain, while for those deformed at 2% it is smaller.

The conclusion from these observations is that the crack initiation and propagation in the late stage of fatigue life occurs under all conditions in the same manner. Hence, for the modeling of the Manson-Coffin law it has no influence.

4.6 Phenomenon caught by this research and the essence clarification

As a summary, the characteristic occurrence of fatigue behavior found in the experimental data can be explained by the dynamic strain aging. A complete solid solution hardening works at 293 K up to 400 K according to literature data,¹⁾ because the dislocation velocities are faster than the diffusion of the carbon atoms. Between 400 K up to 473 K, the dynamic strain aging occur already at low stress levels, because the solid solution of the carbon atom rearrange immediately according to the dislocation movement, in other words DSA happens because of the competition of almost the same velocities of both, the dislocations and the diffusion of the carbon atoms. This was deduced from tension test on cast iron in the range of 423 K~573 K.^{2,3)} At high stress levels, DSA does not occur, because the numbers of dislocations or the dislocation velocities are so high, that the trapped carbon atoms cannot contribute to any hardening effect. At higher temperatures (>573 K) the solid solution hardening mechanism works perfect, because than the carbon diffusion is faster than the dislocations.

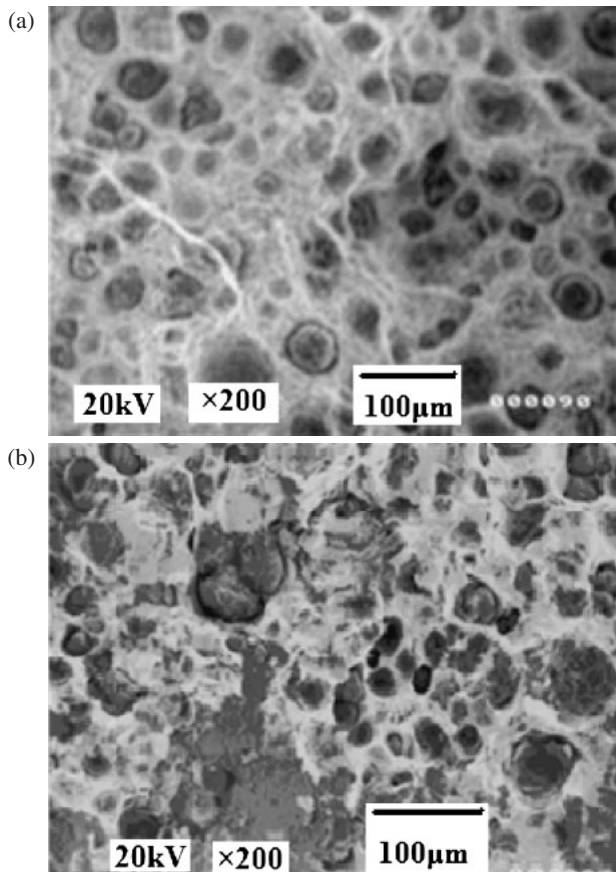


Fig. 9 SEM micrographs of fracture surfaces after low cycle fatigue test with 2% total strain performed at (a) 293 K, (b) 473 K.

The Manson-Coffin rule is based on continuum mechanics and according to the data in the three temperature ranges (293–400 K, 400–573 K, >573 K) different microstructural features occur. So, it is inevitably, that we need three different parameter sets for the materials modeling, which is however sufficient to forecast reliable fatigue

properties. Further research needs to clarify the strain rate dependence.

5. Conclusion

In this research, low cycle fatigue tests at 293 K and 473 K were performed on ferrite ductile cast iron under ambient atmosphere. The obtained results are as following.

- (1) The LCF fatigue life time at high plastic strain rates at 473 K is longer than that at 293 K.
- (2) DSA phenomena occur at high strain in cyclic fatigue tests at 473 K, although it cannot be observed in tensile tests at 473 K.
- (3) The fatigue life time at 473 K is 175 cycles lower than that at 293 K for all stress levels.
- (4) Based on the Manson-Coffin rule, the parameters of the fatigue life time have been determined as $C_p = 0.09$ and 421, $n = 0.65$ and 0.89 for $T = 293$ and 473 K, respectively.

Fatigue behavior of ductile cast iron can be distinguished in three different temperature ranges (293–400 K, 400–573 K, >573 K). When both velocities of dislocation slipping and mass transport of carbon are compatible, as it is the case in the middle temperature range from 400 to 573 K, dynamic strain aging (DSA) occurs. The influence of embrittlement due to large dislocation velocities could also be confirmed.

REFERENCES

- 1) K. Chijiwa and M. Hayashi: *Imono* **51** (2004) 395–400.
- 2) O. Yanagisawa, M. Maruyama, K. Arie, T. Ishigai and M. Konishi: *Imono* **52** (1980) 331–336.
- 3) K. Yasue, H. Matsubara, M. Isotani and Y. Kondo: *Imono* **52** (1980) 669–674.
- 4) M. Hayashi: *Material-Prüfung* **46** (2005) 374–378.
- 5) M. Hayashi and H. Mouri: *J. Solid Mech. Mater. Eng.* **1** (2007) 711–718.
- 6) S. Harada, Y. Akiniwa, T. Ueda and M. Yano: *Trans. Japan Soc. Mechan. Eng.* **62** (1994) 952–959.